Journal of Materials Chemistry A

Accepted Manuscript

ROYAL SOCIETY OF CHEMISTRY

www.rsc.org/materialsA

Journal of Materials Chemistry A

ARTICLE

The Position and Frequency of Fluorine Atoms Changes the Electron Donor/Acceptor Properties of Fluorophenoxy Silicon Phthalocyanines within Organic Photovoltaic Devices

Received 00th January 20xx,
Accepted 00th January 20xx

DOI: 10.1039/x0xx00000x

www.rsc.org/

Benoît H. Lessard,[1,†] Trevor M. Grant,[1] Robin White,[2] Emmanuel Thibau,[2] Zheng-Hong Lu[2] and Timothy P. Bender[1,2,3,*]

In a previous study we have shown the first example of silicon phthalocyanines (SiPcs) applied within organic photovoltaic (OPV) devices. In that study we showed the electronic performance of a SiPc is significantly increased by replacing the axial chloride groups with pentafluoro phenoxy moieties. It was further demonstrated that bis(pentafluoro phenoxy) SiPc (F_{10}-SiPc) is best applied as an electron accepting material within a fullerene-free planar heterojunction (PHJ) OPV. Within this study we have synthesized a new series of fluorophenoxy silicon phthalocyanines ($(XF)_2$-SiPc) whereby the frequency of the fluorine atoms on the fluorophenoxy groups was systematically reduced from 5. These relatively small changes resulted in small changes in UV-vis absorption properties, thermal stability, electrochemical behavior, ultraviolet photoelectron spectroscopy characteristics and solid state arrangement in both single crystals and in thin films obtained by thermal evaporation. Single crystal X-ray diffraction determined that all $(XF)_2$-SiPcs have significantly enhanced π-π interactions compared with dichlorosilicon phthalocyanine (Cl_2-SiPc) and depending on the position and frequency of the fluorine atoms, the solid state arrangement varied significantly. The complete series of $(XF)_2$-SiPcs were then introduced into PHJ OPVs as both electron accepting and electron donating materials when paired with pentacene, α-sexithiophene or C_{60}. It was found that depending on the structure of the $(XF)_2$-SiPcs the most favourable role for the material would either be as an electron donating or electron accepting material and in most cases the $(XF)_2$-SiPcs outperformed Cl_2-SiPc and F_{10}-SiPc. One material, $(246F)_2$-SiPc, did however emerge as one material that has dual functionality. Unoptimized PHJ OPV devices were generally characterized with open circuit voltages (V_{OC}) as high as 0.94 V and power conversion efficiencies > 2.0%. As only the second example of SiPcs being integrated into PHJ OPV devices, these results show that versatile phenoxylation chemistry can impact the application and performance and therefore also demonstrates great promise for this class of significantly understudied organic electronic materials. Finally these results give indications of the direction phenoxy-SiPc molecular design should take in order to potentially further improve their overall performance in PHJ OPV devices.

Introduction

Metal containing phthalocyanines (MPcs) are aromatic macrocycles that bind a single metal atom into their center. Due to their chemical stability, MPcs have found applications in commercial products such as dyes and pigments.[1-6] MPcs have also found application in the expanding filed of organic electronics. For example, MPcs have been utilized as the active layer in organic thin film transistors (OTFTs),[7-10] organic light emitting diodes (OLEDs)[11-13] and organic photovoltaic (OPV) devices.[14-16] By far, the most common MPc used in these applications are divalent MPcs such as zinc MPc (ZnPc) and copper MPc (CuPc).[17-21] To a lesser extent, trivalent metal-containing MPcs such as chloroaluminum MPc (Cl-AlPc)[16,22-24] or chlorogallium MPc (Cl-GaPc)[25,26] have also been applied in OPV devices. However, the use of tetravalent metal and metalloid containing MPcs, such as silicon MPcs[27-29] or tin MPcs[30,31] in organic electronic devices is rare and relatively understudied.

Recently our group has reported the application of tetravalent metal containing MPcs in planar hetero junction (PHJ) OPV devices, both as acceptor and donor layers.[32] Specifically, dichlorosilicon MPc (Cl_2-SiPc) and dichlorogermanium MPc (Cl_2-GePc) where scoped for application as electron donating materials when paired with C_{60} and as electron accepting materials when paired with pentacene or ⍰-sexithiophene (α-6T) where Cl_2-SiPc outperformed Cl_2-GePc in all device configurations.[32] We also synthesized and studied bis(pentafluorophenoxy) SiPc (F_{10}-SiPc), which was found to have similar molecular level opto- and electro-physical characteristics compared to Cl_2-SiPc while having significantly improved π-π stacking between the SiPc molecules in the solid state. F_{10}-SiPc also showed a significant improvement when applied as both an electron acceptor layer or as an electron donor layer in a PHJ OPV device. Improvements where seen in both V_{OC} and J_{SC} resulting (in some cases) an 8-fold increase in overall *PCE* compared to the comparative Cl_2-SiPc containing PHJ OPV devices. It was hypothesized that this increase in performance was a result of two factors: the first is the improved solid-state arrangement due to the

[1]University of Toronto, Department of Chemical Engineering & Applied Chemistry, 200 College Street, Toronto, Ontario M5S 3E5.
[2]University of Toronto, Department of Material Engineering, 200 College Street, Toronto, Ontario M5S 3E5.
[3]University of Toronto, Department of Chemistry, 80 St. George Street, Toronto, Ontario M5S 3H6.
[†]Current Address: University of Ottawa, Department of Chemical and Biological Engineering, 161 Louis Pasteur, Ottawa, Ontario K1N 6N5
*Corresponding author - tim.bender@utoronto.ca

Electronic Supplementary Information (ESI) available: X-ray photoelectron spectroscopy (XPS), scaled absorbance spectra, X-ray crystallography, UV-Vis Photoelectron spectroscopy (UPS) spectra, OPV device characteristics. See DOI: 10.1039/x0xx00000x

addition of pentafluorophenoxy groups, a feature which is well known to play a significant role in the charge transport properties of organic electronic materials.[33-40] Secondly, the steric shielding of the π-electron system due to the addition of pentafluorophenoxy groups that has been reported to reduce the parasitic carrier leakage and charge recombination at the donor/acceptor interface, resulting in a significant increase in V_{OC} usually accompanied by a decrease in J_{SC}.[41-43] These results were in line with our experience with boron subphthalocyanines (BsubPc) whereby the addition of a pentafluorophenoxy group reduced the sublimation temperature, modify the electrochemical properties as well as modify the solid state arrangement of the BsubPc chromaphore.[44-46]

Building on this original study, we targeted the synthesis of several fluorophenoxy SiPc derivatives whereby the position and frequency of the fluorine atoms on the phenoxy fragments were systematically varied in comparison with F_{10}-SiPc. The idea was that this systematic variation would result in differing electrochemical and physical properties as well as modify the solid-state arrangement and thereby alter the overall PHJ OPV device performance. Fluorine atoms are sterically equivalent to hydrogen groups however they are electronically different. Therefore by changing the frequency of fluorine atoms on the phenoxy fragment of the SiPc, we would expect the π-system shielding effect to remain constant while the solid-state arrangement of the molecule would/might vary. These changes could result in PHJ OPVs with similar V_{OC} values to that of F_{10}-SiPc devices but with ranging of J_{SC} values.

Experimental

Materials

3,5-Difluorophenol (98%), 3,4,5-trifluorophenol (97%), 2,4,6-trifluorophenol (99%), 2,3,5,6-tetrafluorophenol (technical grade) were purchased from Oakwood Chemicals, while pentafluorophenol (>99%) and potassium hydroxide (KOH, 85%) were obtained from Sigma-Aldrich. Pentacene (Lumtec, device grade), PEDOT:PSS (Heraeus, Clevios™ P VP Al 4083) and bathocuprione (BCP) (Sigma-Aldrich, 99.6%) were purchased and used as received. Fullerene (C_{60}, SES Research, 99.5%) was purchased and purified once by train sublimation before use. All chemicals were used as received unless otherwise specified. Dichlorosilicon MPc (Cl_2-SiPc) was synthesized according to the literature.[47]

General synthesis of fluorophenoxy SiPc

The synthesis of the fluorophenoxy SiPcs were all performed under similar conditions to that of F_{10}-SiPc as previously reported.[32] In a 100mL three-neck round-bottom flask with a reflux condenser and nitrogen inlet, Cl_2-SiPc (0.5g, 0.82mmol) and 6 molar excess (3x per chloride) fluorophenol (≈5 mmol) were dissolved in chlorobenzene (30 mL). The mixture was stirred and heated at 120 °C under nitrogen for 20 hours. The product was allowed to cool to room temperature and was washed with three successive 165 mL portions of 2M KOH, followed by three successive 165mL portions of water in a separatory funnel. The chlorobenzene was evaporated to give a dark blue powder. Prior to device integration, the samples were purified by train sublimation (≈ 550 ºC / ≈12 h) under vacuum (≈ 40-90 mTorr) using CO_2 as a carrier gas.

Synthesis of bis(3,5-difluorophenoxy) silicon phthalocyanine ($(35F)_2$-SiPc). Yield (before sublimation): 0.548g (83.4%). UV-vis ($CHCl_3$) λ_{max} = 683nm; HRMS [M+] calculated mass: 798.1576, obtained mass: 798.1571. EA: expected wt. %: C(66.16%), H(2.78%) and N(14.03%) - analysis wt. % C(65.71%), H(3.40%) and N(14.43%).

Synthesis of bis(3,4,5-triflurophenoxy) silicon phthalocyanine ($(345F)_2$-SiPc). Yield (before sublimation) 0.566g (82.4%). UV-vis ($CHCl_3$) λ_{max} = 684nm; HRMS [M+] calculated mass: 834.1375, obtained mass: 834.1383. EA: expected wt%: C(63.31%), H(2.41%) and N(13.42%) - analysis wt. %: C(63.07%), H(2.41%) and N(13.50%).

Synthesis of bis(2,4,6-triflurophenoxy) silicon phthalocyanine ($(246F)_2$-SiPc). Yield (before sublimation) 0.560g (82.1%). UV-vis ($CHCl_3$) λ_{max} = 683nm; HRMS [M+] calculated mass: 834.2, obtained mass: 834.2. EA: expected wt. %: C(63.31%), H(2.41%) and N(13.42%) – analysis wt. %: C(63.26%), H(2.38%) and N(13.62%).

Synthesis of bis(2,3,5,6-tetrafluorophenoxy) silicon phthalocyanine ($(2356F)_2$-SiPc). Yield 0.577g (before sublimation) (80.4%). UV-vis ($CHCl_3$) λ_{max} = 686nm; HRMS [M+] calculated mass: 870.1194, obtained mass: 870.1197. EA: expected wt. %: C(66.11%), H(2.78%) and N(14.03%) – analysis wt. %: C(65.71%), H(3.40%) and N(14.43%).

Characterization

Ultraviolet–visible (UV–vis) absorption spectroscopy was performed using PerkinElmer Lambda 1050 with a 10 mm quartz cuvette (solution) or by transmittance of thin films deposited by thermal evaporation onto glass microscope slides. Cyclic voltammetry (CV) was performed using a three-electrode cell assembly at room temperature in a 0.1 M tetrabutylammonium perchlorate (TBAP) in dichloromethane electrolyte solution. The working electrode was a glassy carbon disk electrode, the counter electrode was a polished platinum wire and the reference electrode was Ag/AgCl. An internal standard of bis(pentamethylcyclopentadienyl)iron ($E_{1/2,red}$ = 0.012 V) and a scan rate of 100 mV/s was used for all measurements unless specified otherwise. The samples were bubbled using nitrogen until no dissolved oxygen was present (30-60 minutes prior to each run).

Electronic Device Fabrication and Characterization

Devices were fabricated and characterized in an identical fashion to our recent studies.[24,32,48] For example, 25 mm by 25 mm patterned ITO glass substrates having a sheet resistance of 15 Ω/sq were cleaned by 5 min sonications in detergent in deionized water, pure deionized water, acetone, and then methanol. The substrates were treated with an air-plasma for 5 min followed by a treatment of PEDOT:PSS by spin casting at 500 rpm for 10 seconds followed by 4000 rpm for 30 seconds. The samples were then annealed on a hot plate held at 110 °C for 10 minutes before transfer into the glove box. The substrates were then transferred into a custom vacuum chamber via load lock and transfer arm. The vacuum chamber has a base pressure of ~ 8 x 10^{-8} Torr and the deposition rate were monitored using a quartz crystal microbalance. Manual change of shadow mask by transfer into glove box was performed between the deposition of the BCP and Ag layers. OPV devices of dimensions 2 mm x 10 mm (20 mm^2) were formed from the overlap of the electrode and the ITO region. Voltage sweeps and external quantum efficiencies were obtained under nitrogen atmosphere using simulated solar light supplied by a 300W Xenon Arc lamp with an Air Mass 1.5 Global filter, fed through a Cornerstone™ 260 1/4 m Monochromator with a Keithley 2401 Low Voltage SourceMeter. Light intensity was calibrated with reference to a UV-silicon photodetector. Wavelength scans of the devices were performed

and corresponding currents measured using a Newport Optical Power Meter 2936-R controlled by TracQ Basic software.

Results and discussion

Synthesis of Fluorophenoxy Silicon Phthalocyanine ($(XF)_2$-SiPc) derivatives

A series of fluorophenoxy silicon phthalocyanine ($(XF)_2$-SiPc) were synthesized by the relatively simple reaction of dichloro silicon phthalocyanine (Cl_2-SiPc) with a range of fluorophenols with having between 2 and 4 fluorine atoms positioned in different combinations of ortho, meta and para configurations (**Scheme 1, Table 1**) Each was given a specific designation indicating the position of the fluorine atoms on the fluorophenoxy group. For example $(2356F)_2$-SiPc is bis-2,3,5,6-tetrafluorophenoxy silicon phthalocyanine (see table within **Scheme 1**).

Non-existent gas phase reaction of $(XF)_2$-SiPcs

We previously reported that at elevated temperatures (>350 °C) bis-pentafluorophenoxy silicon phthalocyanine (F_{10}-SiPc) would convert to difluoro silicon phthalocyaninje (F_2-SiPc, **Figure 1**) within the gas phase/under sublimation conditions.[32] While we identified that this reaction could be avoided by increasing the vacuum level and thereby reducing the sublimation temperature, it is generally desirable to avoid gas phase reactions to easily enable device fabricating. Therefore, we began by evaluating the thermal stability of $(XF)_2$-SiPcs.

Similar to the decomposition study performed on F_{10}-SiPc, thermogravimetric analysis (TGA) was used to identify the degree of F_2-SiPc formation for all the $(XF)_2$-SiPcs. The respective wt. % relative to temperature (TGA) traces for F_{10}-SiPc and the $(XF)_2$-SiPcs are illustrated in **Figure 1**. As a point for comparison, the TGA trace for F_{10}-SiPc[32] (**Figure 1A**) clearly shows two sequential mass losses, the first at ≈ 370 °C resulting in a wt. % loss of roughly 22 wt. % which is close to the mass difference between F_{10}-SiPc (906.72 $g{\cdot}mol^{-1}$) and F_2-SiPc (568.61 $g{\cdot}mol^{-1}$) and a second mass loss ≈ 540 °C corresponds to the decomposition of F_2-SiPc. Interestingly, it was observed that for all $(XF)_2$-SiPc (other than F_{10}-SiPc) each experienced only a single mass loss at ≈ 420-440 °C. No mass loss at ≈ 370°C or at ≈ 540°C was observed, suggesting that no (or non above the detection limit) F_2-SiPc was thermally formed for $(35F)_2$-SiPc, $(345F)_2$-SiPc, $(246F)_2$-SiPc or $(2356F)_2$-SiPc. Each was then subsequently purified by train sublimation and the resulting purified products were analysed by mass spectrometry and EA. In all cases, the desired $(XF)_2$-SiPc was identified as the primary component (see experimental section), while in some cases a trace peak at 559.1m/z corresponding to a F-SiPc fragment was present. We hypothesize that this peak is not a result of the sublimation but rather a result of the mass spectrometry technique itself. Elemental analysis was used to confirm that absolute purity of all $(XF)_2$-SiPc samples (experimental section). For example: the obtained EA results for $(35F)_2$-SiPc (EA: expected: C:66.16, H:2.78 and N:14.03 – obtained: C:66.16, H:3.40 and N:14.43) and $(345F)_2$-SiPc (EA: expected: C:63.31, H:2.41 and N:13.42 – obtained: C:63.07, H:2.41 and N:13.50). Finally, to confirm the absence of F_2-SiPc, core level X-ray photoelectron spectroscopy (XPS) was performed on thin films of all $(XF)_2$-SiPc that were deposited under high vacuum by thermal evaporation (similar conditions to OPV device fabrication). The respective spectra can be found in the supporting information (**Figure S1**). Similar to F_{10}-SiPc, all films of $(XF)_2$-SiPc were found to have no F_2-SiPc present (as would be indicated by the presence of an signal for the Si-F bond). In summary, TGA, EA and XPS all confirmed no F_2-SiPc formed when subliming any of $(35F)_2$-SiPc, $(345F)_2$-SiPc, $(246F)_2$-SiPc and $(2356F)_2$-SiPc. Therefore, the use of these $(XF)_2$-SiPc represents a significant improvement in processing variability compared to using F_{10}-SiPc.

Optical and electrochemical characterization of $(XF)_2$-SiPcs

UV-vis absorption spectroscopy was performed on all $(XF)_2$-SiPcs in toluene solution and on thin films deposited on glass by thermal evaporation. The characteristic spectra and tabulation of the respective peak absorbance (λ_{max}) can be found in **Figure S2** (supporting information) and **Table 1**, respectively. As a point for comparison, the characteristics of F_{10}-SiPc and Cl_2-SiPc were also taken from our previous study and included.[32] The optical band gap ($E_{Gap,\ Opt}$) was estimated from the onset of the corresponding absorbance spectra taken from solutions and from thin films (**Table 1**). In addition, the scaled thin film absorption spectrum ($A{\bullet}nm^{-1}$), which was obtained by dividing the measured absorbance by the film thickness (accurately measured using stylus profilometry), can also be found in the supporting information **Figure S3**. The relative absorbance was found to significantly depend on the chemical structure of the $(XF)_2$-SiPc (**Figure S3**).

Cyclic voltammetry (CV) was performed on all the $(XF)_2$-SiPcs and characteristic scans can be found in **Figure 2**. Tabulation of the CV measurements can also be found in **Table 1**. As a comparison, F_{10}-SiPc was also tabulated in **Table 1** and the respective trace can be found elsewhere.[32] It is interesting to note that $(35F)_2$-SiPc (**Figure 2A**) and $(345F)_2$-SiPc (**Figure 2B**) appear to exhibit three distinct reversible reductions and one reversible oxidation, while $(246F)_2$-SiPc (**Figure 2C**) and $(2356F)_2$-SiPc (**Figure 2D**) exhibit only 2 reversible reductions and 1 irreversible oxidation. This observation seems to suggest the importance of the fluorine groups in the *meta*-position in adding an additional reduction event.

These interesting CV results suggest that the energy levels, such as the highest occupied molecular orbital (HOMO) and lowest unoccupied molecular orbital (LUMO) levels, could vary between SiPc derivative based on the nature of the fluorophenoxy fragment. Therefore, ultraviolet and X-ray photoelectron spectroscopy (UPS & XPS) were performed on the $(XF)_2$-SiPcs and the resulting UPS spectra can be found in **Figure S4** along with the tabulated values in **Table 1**. The method in which the UPS and XPS was carried out was identical to that used to characterize F_{10}-SiPc and Cl_2-SiPc in our previous study.[32] Similar to F_{10}-SiPc, the work functions obtained by XPS (not shown) are very similar to those obtained by UPS (Φ_{UPS}) and were found to be equal to 4.3-4.4 eV (**Table 1**). The ionization energy (*IE*) levels were calculated using UPS by adding the valence HOMO offset (Δe), ranging from 1.1-1.4eV from the Fermi to Φ_{UPS}. Therefore, for all $(XF)_2$-SiPcs the *IE* = 5.4 eV to 5.9 eV (**Table 1**). The lowest *IE*s were for both $(35F)_2$-SiPc and $(345F)_2$-SiPc with 5.8 eV and 5.9 eV, respectively. Similar to the electrochemistry, these results suggest a fluorine group in the *meta*-position of the fluorophenoxy fragment is significant and in this case results in a reduction of the *IE*. The transport energy gap, $E_{Gap,T}$, is equal to the $E_{Gap,Opt}$ plus the energy associate to the exciton binding E_{Ex} ($E_{Gap,T} = E_{Gap,Opt} + E_{Ex}$).[49] Both CuPc and Cl-AlPc have previously been characterized by having an $E_{Ex} \approx 0.24$ eV.[50] Therefore, assuming $E_{Ex} \approx 0.24$ eV is similar for all $(XF)_2$-SiPcs we can estimate the $E_{Gap,T}$ (**Table 1**). A visual representation of the Φ_{UPS} and $E_{Gap,T}$ for all the $(XF)_2$-SiPcs can be found in **Figure 3**.

Single Crystals of $(XF)_2$-SiPcs.

In our previous study we showed that the solid state arrangement of F_{10}-SiPc had more significant π-π interactions between the SiPc chromophore than did Cl_2-SiPc and we attributed the increased PHJ OPV device performance to this feature.[32] In this study we therefore sought to characterize the aromatic interactions between SiPc chromophores for all $(XF)_2$-SiPcs. Single crystals of all $(XF)_2$-SiPcs derivatives were grown by slow diffusion of heptane into THF. These single crystals were subsequently diffracted using X-ray crystallography and the resulting thermal ellipsoid plots can be found in **Figure S5** (supporting information). The solid state packing and arrangement of these molecules were analysed and compared against Cl_2-SiPc.[51,52] and F_{10}-SiPc[32]; the results of which are tabulated in **Table S1,** while other information on the obtained crystal diffractions such as density and unit cell size can be found in (**Table S2**). Depending on the nature of the fluorophenoxy fragment a different solid-state arrangement was identified each having a varying degree of interactions between the respective SiPc chromophores (**Figure 4**) For a full discussion on the metrics used to determine the level of π-π interactions see a discussion in the Supporting Information (**Figure S6**).

The sum of these results generally indicate that for all cases, significant increases in the π-π interactions between SiPc chromophores is achieved in the solid-state arrangement when a phenoxy fragment replaces the chloride atom of Cl_2-SiPc molecule. However, depending on the structure of the phenoxy fragment, the position and frequency of the fluorine atoms, the resulting $(XF)_2$-SiPcs have significant differences in both the π-π interactions of the SiPc chromophores and in their overall solid-state arrangement.

Thin Films of $(XF)_2$-SiPcs.

In addition to studying the single crystal X-ray diffraction, power X-ray diffraction (XRD) was performed on thin films of each of the $(XF)_2$-SiPcs deposited by thermal vacuum evaporation onto glass substrates. Characteristic X-ray diffraction patterns for each compound are illustrated in **Figure S8.** The spectra have a generally poor signal to noise ratio but nonetheless, each can be analysed with only one characteristic diffraction peak at 2ϑ = 8.2° - 8.7° corresponding to *d* spacing between 10.1 Å and 10.7 Å for all the $(XF)_2$-SiPcs (**Figure S8A, Table S3**). No appreciable signal was measured for the films of Cl_2-SiPc (**Figure S8)**. A similar single characteristic peak has previously been observed for thin films of other MPcs such as vanadyl MPc (VOPc),[53] magnesium MPc (MgPc)[54] and others.[55,56] While better signal to noise ratio could be obtained by making thicker films and using antireflective surfaces, in our opinion this would result in a response that is no longer representative of the thin films found in our PHJ OPV devices and no longer a useful comparative tool. The characteristic 2ϑ peaks determined experimentally were compared to those predicted from the single crystal X-ray diffractions (**Table S3**). In some cases, such as F_{10}-SiPc, $(2356F)_2$-SiPc and $(35F)_2$-SiPc the difference in 2ϑ is as little as 0.1° - 0.3° while others such as $(345F)_2$-SiPc the difference in 2ϑ is as high as 1.6°. These results suggest that it is possible that the structures of the some $(XF)_2$-SiPcs obtained by X-ray single crystal diffraction are the same as those obtained in thin films by thermal evaporation. However, without more characteristic peaks in the XRD spectra and a better signal to noise ratio it is difficult to say this with certainty. Regardless, these results illustrate that thin films of $(XF)_2$-SiPcs have similar *d* spacing and all are certainly more crystalline than a thin film of Cl_2-SiPc.

AFM was also performed on thin films of $(246)_2$-SiPc, $(35)_2$-SiPc, $(2356)_2$-SiPc and $(345)_2$-SiPc again prepared by thermal vacuum deposition on glass substrates (**Figure S9**) From the AFM measurements we obtained average film roughness (R_A) values which are also included in **Figure S9**. While chemically similar the resulting films have slight differences. For example thin films of $(246)_2$-SiPc where the smoothest with an R_A = 0.243 nm, while thin films of $(2356)_2$-SiPc had a rougher surface with an R_A = 1.908 nm. This trend was also consistent with stylus profilometry analysis performed on the same thin films (**Figure S10**). The XRD and AFM are however potentially inconsistent as the smoothest sample by AFM seemed to be the most crystalline by XRD. Regardless, these results illustrate that the position and frequency of the fluorine atoms of the fluorophenoxy substituents can affect the film morphology, something that will be a point of inquiry moving forward. More specifically, it should be noted again that these films were evaporated onto bare glass substrates and therefore we will look at differing morphologies that may arise depending on the choice of underlying material, as in if the (XF_2)-SiPc is being applied as a donor or an acceptor layer in a PHJ OPV.

Incorporation of $(XF)_2$-SiPcs into PHJ OPV Devices.

Each $(XF)_2$-SiPc was first assessed as an electron donating material by pairing each with the standard electron acceptor material, C_{60}. Each was fabricated into a planar heterojunction (PHJ) OPV device of the following structure: ITO/PEDOT:PSS/$(XF)_2$-SiPc(20 nm)/C_{60}(40 nm)/BCP(7.5 nm)/Ag; the same device configuration we have previous reported using Cl_2-SiPc (device A) and F_{10}-SiPc (device B).[32] Each is plotted as a point of comparison against all devices in the *J-V* curves and external quantum efficiency (EQE) versus wavelength plots illustrated in **Figures 7A** and **7B**, respectively. The device metrics are tabulated in **Table 2**.

In all cases the EQE spectrum show a good spectral coverage and photogeneration originating from both the C_{60} and $(XF)_2$-SiPc layers (**Figure 5B**). The OPV devices made using $(XF)_2$-SiPcs were also found to have an elevated V_{OC} of 0.77 V - 0.94 V, which is greater than device made using Cl_2-SiPc (V_{OC} = 0.24) and generally greater than that of F_{10}-SiPc (V_{OC} = 0.76). As a further point of comparison, these measured V_{OC} values are also greater than those obtained by our group (V_{OC} = 0.67)[24] and others (V_{OC} = 0.26 - 0.84)[16,22,23] for the pairing of C_{60} with chloroaluminum phthalocyanine (Cl-AlPc), a well-studied electron donating material, used in PHJ OPV devices. For a better comparison, bar graphs comparing the obtained V_{OC} to the J_{SC} can be found in **Figure 6**.

The device metrics clearly indicate that $(246F)_2$-SiPc, $(2356F)_2$-SiPc, $(345F)_2$-SiPc, $(35F)_2$-SiPc outperform the previously reported F_{10}-SiPc[32] (**Table 2**, **Figure 5**). However, we were not able to determine a clear trend/structure-property relationship between the solid state arrangements or electrochemical properties of the $(XF)_2$-SiPc and the resulting device characteristics.

It has been suggested that the $V_{OC} = Ig \approx E_{HOMO}$ (donor layer) – E_{LUMO} (acceptor layer).[57,58] Therefore as a comparison, bar graphs plotting the obtained V_{OC} versus the calculated *Ig* can be found in the supporting information (**Figure S11**). This plot shows that some $(XF)_2$-SiPc containing PHJ OPVs, such as the ones based on $(246F)_2$-SiPc, $(2356F)_2$-SiPc, follow this trend, others do not. In attempts to find a trend between the $(XF)_2$-SiPc structures and device metrics, several other comparisons were considered (**Figure S12-S13**): V_{OC} relative to crystal density; molar crystal density; *Ig* and the Δ LUMO (difference in LUMO energy level between donor and acceptor layer). Similarly to the *Ig* vs. V_{OC} plots no conclusive correlation is observed.

Recently, several studies have explored the effect of π-system shielding and its effect on the device V_{OC}. [41,43,59] We hypothesized that this was one of the reasons for the increased device

performance for F_{10}-SiPc relative to Cl_2-SiPc.[32] Therefore, the angle or distance between the fluorophenoxy groups and the respective SiPc molecules for the $(XF)_2$-SiPcs were compared to the device V_{OC}, however, again no definitive correlation was identified (**Figure S12**). Finally, the normalized absorbance of the $(XF)_2$-SiPcs was compared to the device J_{SC} and again no correlation was found (**Figure S13**). Regardless, when paired with C_{60}, the addition of any fluorophenoxy group to SiPc results in improved PHJ OPV device characteristics compared to Cl_2-SiPc and F_{10}-SiPc. These results suggest that $(246F)_2$-SiPc, $(2356F)_2$-SiPc, $(345F)_2$-SiPc and $(35F)_2$-SiPc are all superior electron donor molecules when paired with C_{60}. These results also suggest that, when paired with C_{60}, $(246F)_2$-SiPc is the best candidate out of all the fluorophenoxy SiPcs (**Table 2**, **Figure 5**).

Secondly, we studied the application of $(XF)_2$-SiPcs as electron acceptor layers when paired with pentacene using the following device configuration: ITO/PEDOT:PSS/pentacene(43 nm)/ $(XF)_2$-SiPcs(40 nm)/BCP(11 nm)/Ag (**Table 2**); $(2356F)_2$-SiPc (device I), $(345F)_2$-SiPc (device J), $(246F)_2$-SiPc (device K), $(35F)_2$-SiPc (device L). In all these cases the same device configuration was employed to facilitate the comparison of the $(XF)_2$-SiPcs to our previously reported devices incorporating Cl_2-SiPc (device G) and F_{10}-SiPc (device H).[32] (**Figure 7A** and **B**, **Table 2**). For a better visual comparison, bar graphs comparing the obtained V_{OC} to the J_{SC} can be found in **Figure 6C** and **D**. Of note, $(2356F)_2$-SiPc, $(345F)_2$-SiPc, $(246F)_2$-SiPc and $(35F)_2$-SiPc all experience a reduced J_{SC} and increased V_{OC} compared Cl_2-SiPc and F_{10}-SiPc (**Figure 7A**, **Table 2**).

When examining the EQE spectra (**Figure 7B**) it becomes apparent that the majority of the photogeneration is taking place in the $(XF)_2$-SiPc layer as evidenced by the peaks between 600 - 800 nm 300 - 400nm, whereas very little EQE contribution in the 400 - 700 nm region, corresponding to the pentacene layer, is present. Previously, we identified that both Cl_2-SiPc and F_{10}-SiPc when paired with pentacene could facilitate the triplet harvesting from the pentacene layer resulting in a drop in V_{OC} and increase in J_{SC}.[32] All $(XF)_2$-SiPcs LUMO levels are lower than -3.8 eV, which is consistent with previous reported electron acceptors that can effectively dissociate pentacene triplets.[78,79] However, it appears that little triplet harvesting is taking place in $(2356F)_2$-SiPc, $(345F)_2$-SiPc, $(246F)_2$-SiPc and $(35F)_2$-SiPc layers of the respective PHJ OPV devices (**Figure 7B**). Similar to the OPV devices made using C_{60}, attempts at correlating the device J_{SC} to scaled absorbance, the device V_{OC} to crystal density, molar crystal density, *Ig* and delta LUMO can be found in the supporting information.

Given the poor photogeneration from pentacene and in order to avoid entirely the singlet fission/triplet harvesting process, a 60 nm layer of α-sexithiophene (α-6T) was also used as a donor layer and paired with 20 nm of all the $(XF)_2$-SiPcs (device O to R). The resulting PHJ OPV device characteristics can be found in **Table 2** and **Figure 7C** and **D**. As a comparison PHJ OPV devices containing Cl_2-SiPc (device M) and F_{10}-SiPc (Device N) were taken from the literature and added to both **Table 2** and **Figure 7**.[32] Unlike the pentacene case, two distinct contributions corresponding to the absorption of α-6T and $(XF)_2$-SiPc are both found in the EQE spectra of all $(XF)_2$-SiPc PHJ OPV devices (**Figure 7D**). In all cases, $(246F)_2$-SiPc, $(2356F)_2$-SiPc, $(345F)_2$-SiPc and $(35F)_2$-SiPc were found to have an elevated V_{OC} of 0.56 V - 0.68 V compared to both Cl_2-SiPc (V_{OC} = 0.29) and F_{10}-SiPc (V_{OC} = 0.41). In most cases the J_{SC} was found be similar between devices regardless of the $(XF)_2$-SiPc used as an electron acceptor, except when using $(345F)_2$-SiPc that resulted in roughly 2 fold increase in J_{SC} when compared to the other $(XF)_2$-SiPcs and a 4 fold increase when compared to Cl_2-SiPc (**Table 2**, **Figure 7**).

Bar graphs comparing the obtained V_{OC} to the J_{SC} can be found in **Figure 6**. Again no definite structure-property correlation could be identified between base material properties and devices characteristics (**Figure S11-S12**). That being said, when compared to Cl_2-SiPc and F_{10}-SiPc, the device metrics do demonstrate that $(246F)_2$-SiPc, $(2356F)_2$-SiPc, $(345F)_2$-SiPc and $(35F)_2$-SiPc are all superior electron acceptor molecules when paired with α-6T and that they also function better with α-6T than with pentacene. The device metrics also suggest that, when paired with α-6T, $(345F)_2$-SiPc (device P) is the best candidate out of all the $(XF)_2$-SiPcs when considering only J_{SC}.. However, given J_{SC} is largely a device metric and not a metric directly attributable to a material, it is interesting to note that $(246F)_2$-SiPc again shows the highest V_{OC} as it did when paired with C_{60} as an electron donor.

When examining the EQE spectra it also becomes apparent that the majority of the photogeneration is taking place in the α-6T layer as evidenced by the higher EQE contribution between 300 – 550 nm compared with that of the SiPc contribution between 550 – 750 nm. So that being said, despite the good performance of $(345F)_2$-SiPc (device P) significant imbalances in the photogeneration between the contributions from the α-6T layer and the $(345F)_2$-SiPc layer (**Figure 7D**) should be addressed in future studies with further device engineering of the respective layer thicknesses and the PHJ OPVs as a whole.

To summarize, three sets of PHJ OPV devices were used to initially scope this new series of $(XF)_2$-SiPcs and to identify their function as electron acceptor layers and/or as electron donor layers in PHJ OPVs; two candidates have emerged. When paired with α-6T, $(345F)_2$-SiPc is the best candidate electron acceptor if one considers only the J_{SC}. However, if V_{OC} is considered, a property more attributable directly to the material, $(246F)_2$-SiPc stands out with the highest V_{OC} when paired with α-6T. This is similar as to when $(246F)_2$-SiPc is paired with C_{60}, whereby it was shown to be the best candidate donor layer of all the $(XF)_2$-SiPcs. Therefore, to confirm, we fabricated repeated replicates (3 sets of 16-20 devices) of these candidate materials within their respective PHJ OPVs and the above reported data reflects these replicates (**Figure 5** and **Figure 7**).

While these PHJ OPV devices are unoptimized (only one thickness studied) and the results clearly indicate that the functionality of SiPcs as organic electronic materials, and that their respective functionality can be effected through chemistry at the axial position.

Independent of further device optimization to achieved enhanced J_{SC}, we believe the results outline design rules for the next molecular design iteration of SiPcs for application in PHJ OPV devices. Particular noteworthy is $(246F)_2$-SiPc which has stood out as having the highest V_{OC} when applied as both an electron donor and an electron acceptor. The UPS and electrochemical data ($E_{1/2,red}$) acquired for $(246F)_2$-SiPc is consistent with what the Hammett parameters for *ortho*- and *para*-fluorine substituents would predict, that the 2,4,6-trifluorophenoxy axial substituents have the least electron withdrawing effect of all the $(XF)_2$-SiPc phenoxy substituents studied. The result is therefore a compound with the highest HOMO level and more generally this indicates the electron withdrawing or donating character of the phenoxy group does indeed effect the SiPc π-electron system and the resulting V_{OC} of the PHJ OPV devices. Therefore, moving forward we will study phenoxy-SiPcs devoid of fluorine groups to ascertain whether electron-neutral (hydrogens) or electron-donating, such as *para*- and *ortho*-methyl groups, may further raise the HOMO of the

phenoxy-SiPcs and increase the V_{OC} of the resulting PHJ OPVs while still providing the π-shielding effect. Raising the HOMO will of course result is smaller offset with α-6T and a larger offset with C_{60}, so synthesis and device incorporation is clearly required to confirm this hypothesis and the molecular design pathway.

Conclusions

A series of fluorophenoxy silicon phthalocyanines ($(XF)_2$-SiPcs) with ranging frequencies and positions of fluorine atoms on the fluorophenoxy molecular fragments were synthesized and fully characterized. Each was incorporated into planar heterojunction organic photovoltaic (PHJ OPV) devices as both electron accepting and electron donating layers. None of the $(XF)_2$-SiPcs exhibited the previously observed thermal decomposition into F_2-SiPc during sublimation. The characterization of the $(XF)_2$-SiPcs revealed small variations in UV-Vis absorption properties, thermal stability, electrochemical characteristics, ultraviolet photoelectron spectroscopy characteristics, single crystal X-ray diffractions, powder X-ray diffraction and AFM of thin films. In all cases, the $(XF)_2$-SiPc had increased π-π interactions between neighboring SiPc chromophores compared to Cl_2-SiPc.

A series of PHJ OPV devices were fabricated using $(XF)_2$-SiPcs paired with pentacene, α-6T or C_{60}. The use of $(XF)_2$-SiPcs with α-6T or C_{60} resulted in devices that outperformed previously reported Cl_2-SiPc and F_{10}-SiPc based devices. When the $(XF)_2$-SiPcs were paired with C_{60} the device with the greatest overall efficiency (*PCE*) was device E, which employed $(246F)_2$-SiPc resulting in V_{OC} = 0.87 ± 0.03 V, J_{SC} = 4.6 ± 0.4 mA·cm^{-2}, *FF* = 0.44 ± 0.02 and a *PCE* = 1.8 ± 0.2 % (**Table 2**) outperforming our previously studied Cl_2-SiPc and F_{10}-SiPc.[32] While these devices are unoptimized (only one thickness of $(XF)_2$-SiPcs studied), we now have demonstrated that the use of SiPcs results in PHJ OPV devices that are on par and even outperforming devices made using well optimized and well-studied Cl-AlPc/C_{60}[16,23-25,60] and CuPc/C_{60}[16,18,19,61].

Conversely, when paired with pentacene all the devices using $(XF)_2$-SiPcs resulted in devices greater V_{OC}s but smaller J_{SC}s compared to the use of Cl_2-SiPc and F_{10}-SiPc. The EQE spectra indicated that the majority of the photogeneration is taking place in the $(XF)_2$-SiPc layer unlike for Cl_2-SiPc and F_{10}-SiPc.

When paired with α-6T, the greatest efficiency was obtained using $(345F)_2$-SiPc (device P, **Table 2**) resulting in devices characterized by having V_{OC} = 0.66 ± 0.09 V, J_{SC} = 3.5 ± 0.4 mA·cm^{-2}, *FF* = 0.43 ± 0.08 and a *PCE* = 1.0 ± 0.2%. While a few examples are emerging in the literature indicating the use of MPcs as electron acceptor layers in fullerene-free OPV devices they are still relatively rare[24,32,62,63] and therefore this study suggest the potential role SiPcs can play in this space.

Ultimately, this study has identified two candidate SiPc materials $(345F)_2$-SiPc and $(246F)_2$-SiPc for use as electron acceptor and electron donating materials in PHJ OPV devices (respectively). These two candidates are stated based on complete PHJ OPV device efficiencies. If V_{OC}s are considered, $(246F)_2$-SiPc stands out as a candidate in each application. The idea that 2,4,6-trifluorophenoxy is the least electron withdrawing phenoxy fragment studied implies that future studied and molecular designs should consider electron-neutral or electron-donating substituents on the phenoxy fragment to potentially further enhance the V_{OC} of the resulting PHJ OPV devices.

Acknowledgements

We would like to acknowledge the kind discussions with Prof Yun Chi (National Tsing Hua University, Taiwan) regarding these results which occurred at the 3rd Reciprocal WIN-Taiwan Nanotechnology Workshop at the University of Waterloo (Waterloo, Ontario, Canada) from August 4-7 2015.

This work was supported by a Natural Sciences and Engineer Research Council (NSERC) Banting Post-Doctoral fellowship to BHL and a Discovery Grant to TPB. Queen Elizabeth II Graduate Scholarships in Science and Technology (QEII-GSST) helped support RTW. The authors would also like to acknowledge financial support from Saudi Basic Industries (SABIC). We would also like to thank Dr. Alan Lough (Department Chemistry, University of Toronto) and Dr. George Kretschmann (Department Geology, University of Toronto) for their help with the X-ray crystallography diffraction of single crystals and of thin films, respectively.

References

1 Listigovers, N. A.; Allen, C. G.; Martin, T. I.; Hamer, G. K.; Hsiao, C. K.; Baranyi, G. U.S. Patent US 5,521,043, May 28 1996.
2 Giambalvo, V. A.; Somerville, N. J. U.S. Patent US 2,526,345, Oct. 17 1950.
3 Funatsu, T.; Inuzuka, Y.; Mishina, T.; Kitamura, K.; Chiba, A. U.S. Patent US 4,221,606, Sep. 9 1980.
4 Alfred, S.; Summit, N. J. U.S. Patent US 2,861,005, Nov. 18 1958.
5 Eastes, J. W.; Somerville, N. J. U.S. Patent US 2,770,629, Nov. 13 1956.
6 la Torre, de, G.; Claessens, C. G.; Torres, T.. *Chem. Commun.* **2007**, 2000–2015.
7 Roberts, M. E.; Sokolov, A. N.; Bao, Z. *J. Mater. Chem.* **2009**, *19*, 3351–3363.
8 Tang, W. M.; Ng, W. T.; Greiner, M. T.; Qiu, J.; Helander, M. G.; Lu, Z.-H. *J. Vac. Sci. Technol. B* **2013**, *31*, 0122011–0122016.
9 Li, X.; Jiang, Y.; Xie, G.; Tai, H.; Sun, P.; Zhang, B. *Sens. Actuators B* **2013**, *176*, 1191–1196.
10 Melville, O.; Lessard, B. H.; Bender, T. P.. *ACS Appl. Mater. Interfaces* **2015**, *7*, 13105–13118.
11 Deng, Z.; Lu, Z.; Chen, Y.; Yin, Y.; Zou, Y.; Xiao, J.; Wang, Y.. *Solid-State Electron.* **2013**, *89*, 22–25.
12 Wang, H.; Ji, Z.; Liu, M.; Shang, L.; Liu, G.; Liu, X.; Liu, J.; Peng, Y. *Sci. China Ser. E-Technol. Sci.* **2009**, *52*, 3105–3116.
13 Hou, J.; Guo, X. *Organic Solar Cells*; Green Energy and Technology; Springer London: London, 2012; pp. 17–42.
14 Chen, Y.-C.; Hsu, C.-Y.; Lin, R. Y.-Y.; Ho, K.-C.; Lin, J. T. *ChemSusChem* **2013**, *6*, 20–35.
15 Xue, J.; Uchida, S.; Rand, B.; Forrest, S. *Appl. Phys. Lett.* **2004**, *84*, 3013–3015.
16 Kim, D. Y.; So, F.; Gao, Y. *Sol. Energy Mater. Sol. Cells* **2009**, *93*, 1688–1691.
17 Williams, G.; Sutty, S.; Klenkler, R.; Aziz, H. *Sol. Energy Mater. Sol. Cells* **2014**, *124*, 217–226.
18 Chen, W.-B.; Xiang, H.-F.; Xu, Z.-X.; Yan, B.-P.; Roy, V. A. L.; Che, C.-M.; Lai, P.-T. *Appl. Phys. Lett.* **2007**, *91*, 191109–191109–3.
19 Kumar, H.; Kumar, P.; Bhardwaj, R.; Sharma, G. D.; Chand, S.; Jain, S. C.; Kumar, V. *J. Phys. D: Appl. Phys.* **2008**, *42*, 015103.
20 Zhou, Y.; Taima, T.; Miyadera, T.; Yamanari, T.; Kitamura, M.; Nakatsu, K.; Yoshida, Y. *Appl. Phys. Lett.* **2012**, *100*, 233302.
21 Jin, F.; Chu, B.; Li, W.; Su, Z.; Zhao, B.; Zhang, T.; Yan, X. *Org. Electron.* **2013**, *14*, 1130–1135.

22 Yoshida, K.; Oku, T.; Suzuki, A.; Akiyama, T. *Adv. Chem. Eng. Sci.* **2012**.
23 Chauhan, K. V.; Sullivan, P.; Yang, J. L.; Jones, T. S. *J. Phys. Chem. C* **2010**, *114*, 3304–3308.
24 Lessard, B.; Mohammad, A.; Grant, T. M.; White, R.; Lu, Z.-H.; Bender, T. P. *J. Mater. Chem.* **2015**, *3*, 5047–5053.
25 Yuen, A. P.; Jovanovic, S. M.; Hor, A.-M.; Klenkler, R. A.; Devenyi, G. A.; Loutfy, R. O.; Preston, J. S. *Sol. Energy* **2012**, *86*, 1683–1688.
26 Yuen, A. P.; Bamsey, N. M.; Hor, A.-M.; Preston, J. S.; Klenkler, R. A.; Jovanovic, S. M.; Loutfy, R. O. *Sol. Energy Mater. Sol. Cells* **2011**, *95*, 3137–3141.
27 Lessard, B. H.; Dang, J. D.; Grant, T. M.; Gao, D.; Seferos, D. S.; Bender, T. P. *ACS Appl. Mater. Interfaces* **2014**, *6*, 15040–15051.
28 Honda, S.; Nogami, T.; Ohkita, H.; Benten, H.; Ito, S. *ACS Appl. Mater. Interfaces* **2009**, *1*, 804–810.
29 Honda, S.; Ohkita, H.; Benten, H.; Ito, S. *Adv. Energy Mater.* **2011**, *1*, 588–598.
30 Du, C.; Yu, J.; Huang, J.; Jiang, Y. Organic Solar Cells Using Tin (II) Phthalocyanine as Donor Material. *Energy Procedia* **2011**, *12*, 519–524.
31 Song, D.; Wang, H.; Zhu, F.; Yang, J.; Tian, H.; Geng, Y.; Yan, D. *Adv. Mater.* **2008**, *20*, 2142–
32 Lessard, B. H.; White, R. T.; Al-Amar, M.; Plint, T.; Castrucci, J. S.; Josey, D.; Lu, Z. H.; Bender, T. P. *ACS Appl. Mater. Interfaces* **2015**, *7*, 5076–5088.
33 Anthony, J. E.; Eaton, D. L.; Parkin, S. R.. *Org. Lett.* **2002**, *4*, 15–18.
34 Anthony, J. E.; Brooks, J. S.; Eaton, D. L.; Parkin, S. R. *J. Am. Chem. Soc.* **2001**, *123*, 9482–9483.
35 Sheraw, C. D.; Jackson, T. N.; Eaton, D. L.. *Adv. Mater.* **2003**, *15*, 2009–2011.
36 Payne, M. M.; Delcamp, J. H.; Parkin, S. R.; Anthony, J. E. *Org. Lett.* **2004**, *6*, 1609–1612.
37 Payne, M. M.; Parkin, S. R.; Anthony, J. E. *J. Am. Chem. Soc* **2005**, *127*, 8028–8029.
38 Payne, M. M.; Parkin, S. R.; Anthony, J. E.; Kuo, C.-C.; Jackson, T. N. *J. Am. Chem. Soc* **2005**, *127*, 4986–4987.
39 Meng, H.; Sun, F. P.; Goldfinger, M. B.; Jaycox, G. D.; Li, Z. G.; Marshall, W. J.; Blackman, G. S. *J. Am. Chem. Soc.* **2005**, *127*, 2406–2407.
40 Anthony, J. E. *Chem. Rev* **2006**, *106*, 5028–5048.
41 Schlenker, C. W.; Barlier, V. S.; Chin, S. W.; Whited, M. T.; McAnally, R. E.; Forrest, S. R.; Thompson, M. E. *Chem. Mater* **2011**, *23*, 4132–4140.
42 Beljonne, D.; Cornil, J.; Muccioli, L.; Zannoni, C.; Brédas, J.-L.; Castet, F. E. *Chem. Mater* **2011**, *23*, 591–609.
43 Erwin, P.; Thompson, M. E. *Appl. Phys. Lett.* **2011**, *98*, 223305.
44 Morse, G. E.; Helander, M. G.; Maka, J. F.; Lu, Z.-H.; Bender, T. P. *ACS Appl. Mater. Interfaces* **2010**, *2*, 1934–1944.
45 Castrucci, J. S.; Helander, M. G.; Morse, G. E.; Lu, Z.-H.; Yip, C. M.; Bender, T. P. *Cryst Growth Des* **2012**, *12*, 1095–1100.
46 Morse, G. E.; Helander, M. G.; Stanwick, J.; Sauks, J. M.; Paton, A. S.; Lu, Z.-H.; Bender, T. P. *J. Phys. Chem. C* **2011**, *115*, 11709–11718.
47 Lowery, M. K.; Starshak, A. J.; Esposito, J. N.; Krueger, P. C.; Kenney, M. E. *Inorg Chem* **1965**, *4*, 128–128.
48 Josey, D. S.; Castrucci, J. S.; Dang, J. D.; Lessard, B. H.; Bender, T. P. *ChemPhysChem* **2015**, *16*, 10.1002–cphc.201402751.
49 Hill, I. G.; Kahn, A.; Soos, Z. G.; Pascal, R. A., Jr. *Chem. Phys. Lett.* **2000**, *327*, 181–188.
50 Cho, S. W.; Piper, L. F. J.; DeMasi, A.; Preston, A. R. H.; Smith, K. E.; Chauhan, K. V.; Sullivan, P.; Hatton, R. A.; Jones, T. *J. Phys. Chem. C* **2010**, *114*, 1928–1933.
51 Kojima, Y.; Osano, Y. T.; Ohashi, T.. *Bull. Chem. Soc. Jpn.* **2000**, *73*, 2469–2475.
52 Silver, J.; Frampton, C. S.; Fern, G. R.; Davies, D. A.; Miller, J. R.; Sosa-Sanchez, J. L. *Inorg Chem* **2001**, *40*, 5434–5439.
53 Basova, T. V.; Kiselev, V. G.; Dubkov, I. S.; Latteyer, F.; Gromilov, S. A.; Peisert, H.; Chasse, T. *J. Phys. Chem. C* **2013**, *117*, 7097–7106.
54 El-Nahass, M. M.; Atta, A. A.; El-Sayed, H. E. A.; El-Zaidia, E. F. M. *App. Surf. Sci.* **2008**, *254*, 2458–2465.
55 Pirriera, Della, M.; Puigdollers, J.; Voz, C.; Stella, M.; Bertomeu, J.; Alcubilla, R. *J. Phys. D: Appl. Phys.* **2009**, *42*, 145102.
56 Schuenemann, C.; Elschner, C.; Levin, A. A.; Levichkova, M.; Leo, K.; Riede, M. *Thin Solid Films* **2011**, *519*, 3939–3945.
57 Rand, B.; Burk, D.; Forrest, S. *Phys. Rev. B* **2007**, *75*, 115327–115311.
58 Mutolo, K. L.; Mayo, E. I.; Rand, B. P.; Forrest, S. R.; Thompson, M. E. *J. Am. Chem. Soc* **2006**, *128*, 8108–8109.
59 Yang, L.; Zhou, H.; You, W. *J. Phys. Chem. C* **2010**, *114*, 16793–16800.
60 Bailey-Salzman, R. F.; Rand, B. P.; Forrest, S. R. *Appl. Phys. Lett.* **2007**, *91*, 013508.
61 Brumbach, M.; Placencia, D.; Armstrong, N. R. *J. Phys. Chem. C* **2008**, *112*, 3142–3151.
62 Beaumont, N. L. Investigating New Materials and Understanding the Ambipolar Qualities of Organic Small Molecules for Use in Organic Photovoltaics, The university of Warwick, 2013.
63 Beaumont, N.; Castrucci, J. S.; Sullivan, P.; Morse, G. E.; Paton, A. S.; Lu, Z.-H.; Bender, T. P.; Jones, T. S. *J. Phys. Chem. C* **2014**, *118*, 14813–14823.

Journal of Materials Chemistry A

ARTICLE

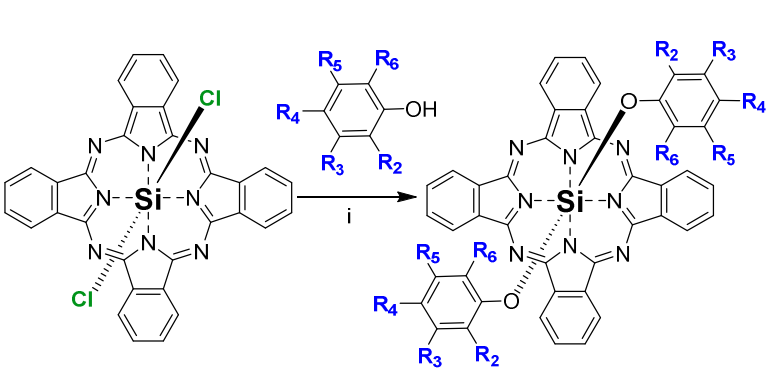

$(2356F)_2$-SiPc	$(246F)_2$-SiPc
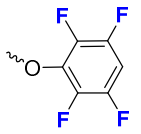	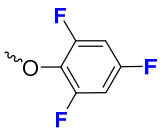
$(345F)_2$-SiPc	$(35F)_2$-SiPc
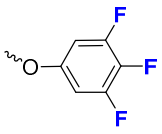	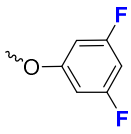

Scheme 1. Synthetic route and chemical structure of fluorophenoxy silicon phthalocyanines (XF_2-SiPc) used in this study. Conditions: (i) 6 molar equivalents of fluorophenol; 120 °C, chlorobenzene, 20 hrs.

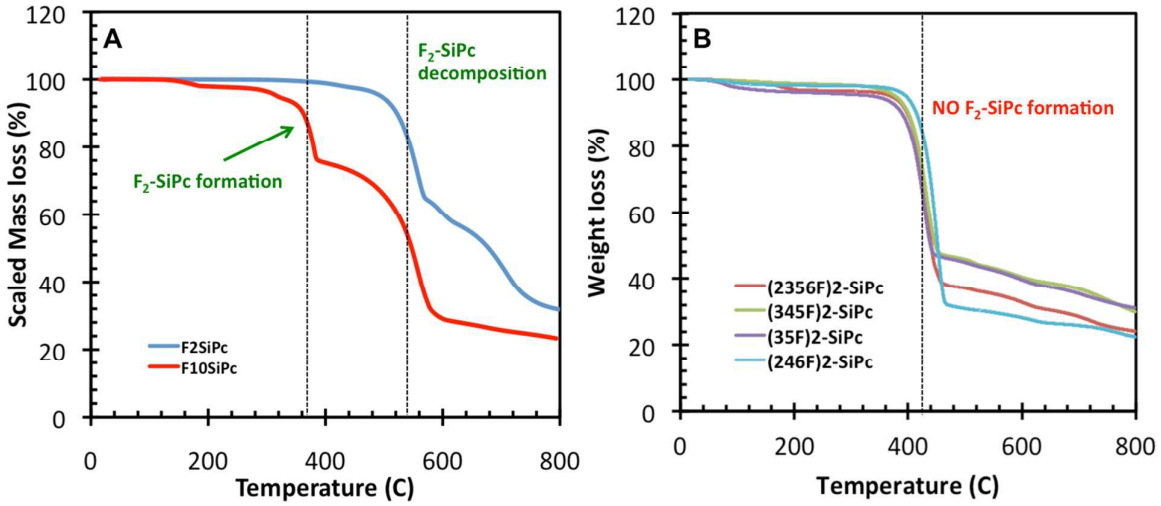

Figure 1. Thermogravimetric analysis (TGA) of fluorophenoxy silicon phthalocyanines ($(XF)_2$-SiPcs). An initial mass of 5-15 mg and a heating rate of 5 °C·min^{-1} was employed for all the runs. The phenoxy SiPcs molecular structures and characterization can be found in **Figure 1** and **Table 1**, respectively.

Journal of Materials Chemistry A

ARTICLE

Table 1. UV-Vis absorbance and electrochemical and X-ray/ultraviolet photoelectron spectroscopy characteristics of functional silicon phthalocyanines (SiPc).

	Toluene		Films			DCM				Films			
Sample	λ_{MAX} [a] (nm)	$E_{Gap,OPT}$ [b] (eV)	λ_{MAX} [a] (nm)	$E_{Gap,OPT}$ [b] (eV)	$E_{Gap,T}$ [c]	$E_{OX,peak}$ (V)	$E_{Red,peak}$ (V)	$E_{OX,1/2}$ (V)	$E_{Red,1/2}$ (V)	Φ_{UPS} [d] (eV)	Δe (eV)	$IE_{,UPS}$ (eV)	*Ref.*
Cl_2-SiPc	685	1.77	752	1.56	1.80	1.27*	-0.68, -1.07	-	-0.62, -1.02	4.1	1.6	5.7	[32]
F_{10}-SiPc	686	1.73	737	1.62	1.86	1.26	-0.43, -0.88	1.22	-0.46, -0.91	4.4	1.4	5.7	[32]
$(2356F)_2$-SiPc	686	1.77	725	1.66	1.90	0.88*	-0.52*,-0.88, -1.24,-1.49*	-	-0.50*,-0.83, -1.19	4.4	1.3	5.7	This work
$(246F)_2$-SiPc	683	1.78	721	1.61	1.85	1.20*	-0.59*, -0.93, -1.29	-	-0.56*, -0.88, -1.24	4.4	1.1	5.4	This work
$(345F)_2$-SiPc	684	1.78	713	1.61	1.85	1.29	-0.51, -0.90, -1.26, -1.57*	1.24	-0.48, -0.83, -1.19	4.4	1.4	5.9	This work
$(35F)_2$-SiPc	683	1.78	736	1.65	1.89	1.27*	-0.52, -0.88, -1.24, -1.51*	-	-0.45, -0.83, -1.19	4.3	1.4	5.8	This work

[a] λ_{MAX} was determined as the peak wavelength of the absorbance spectra
[b] $E_{Gap,Opt}$ was determined from the onset of the absorbance spectra (Figure 2)
[c] $E_{Gap,T} = E_{Gap,Opt} + E_{Ex}$.[49] Where $E_{Ex} \approx 0.24$eV[50]
[d] Work Function (Φ) determined by ultraviolet photoelectron spectroscopy (UPS) and confirmed by X-ray photoelectron spectroscopy (XPS)
*Denotes that the peak was irreversible or very small compared to the other peaks and that the software did not pick up the peak through all three runs.

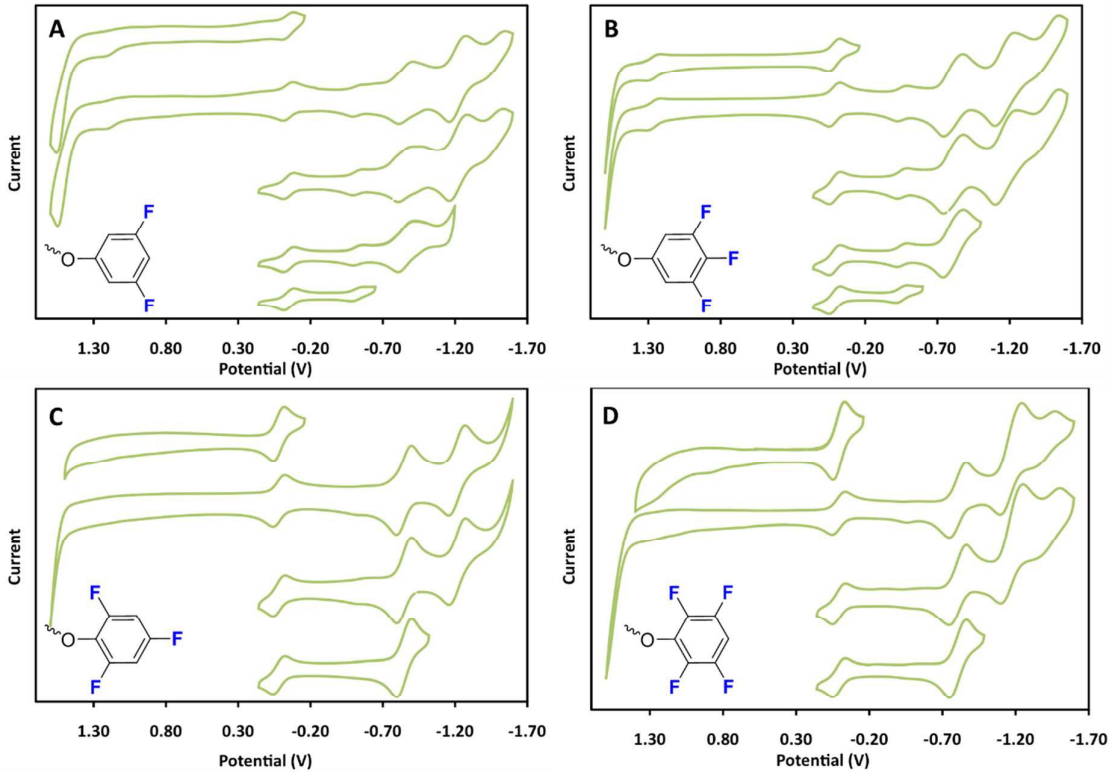

Figure 2 – Characteristic cyclic voltammograms of (b) $(35F)_2$-SiPc; (**B**) $(345F)_2$-SiPc; (**C**) $(246F)_2$-SiPc and (**D**) $(2356F)_2$-SiPc vs. Ag/AgCl using a working electrode of glassy carbon, a platinum wire counter electrode and an internal standard of bis(pentamethyl cyclopentadienyl)iron ($E_{1/2}$ = -0.012 V). All scans are an average of three runs using a scan rate of 100mV/s. Identified peaks and half-wave potentials can be found in **Table 1**.

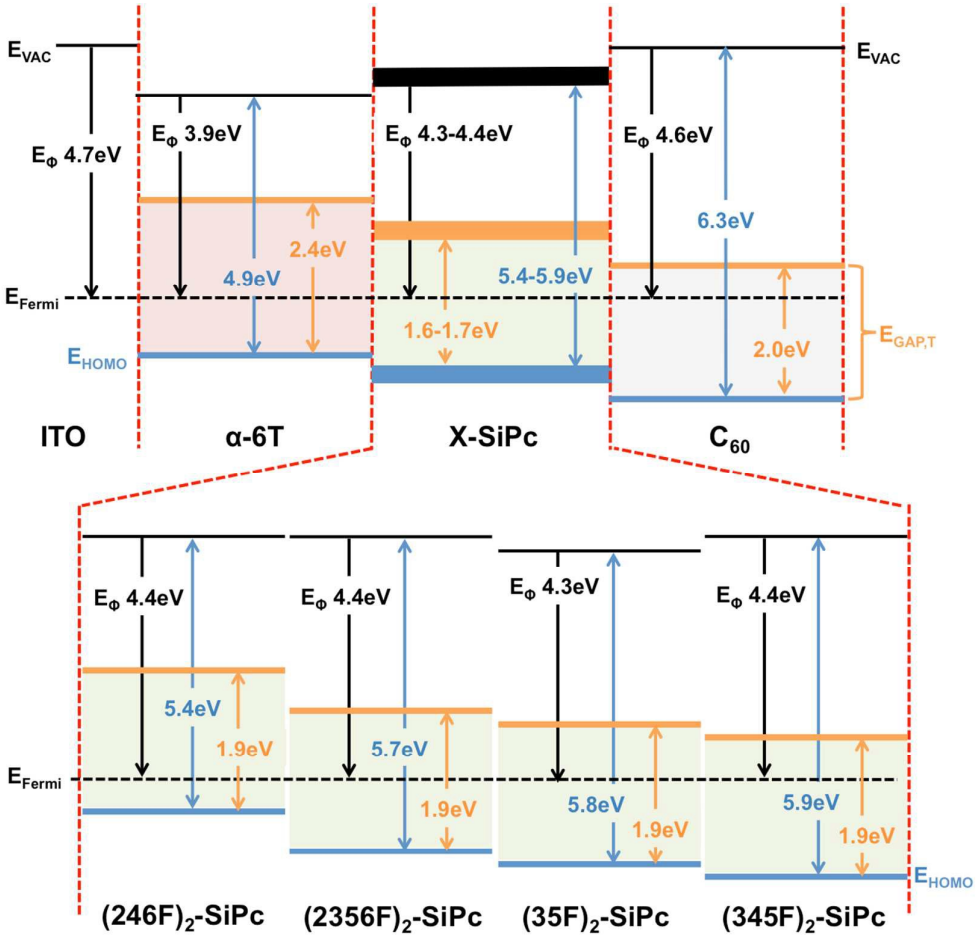

Figure 3. Schematic view of the E_{HOMO} levels and local vacuum level shifts for ITO, $(XF)_2$-SiPcs, C_{60} and α-6T. For comparison the Fermi energy levels were all assumed to be equal. For the X-SiPc, the E_{HOMO} levels were obtained by UPS and the $E_{GAP,T} = E_{Gap,Opt} + E_{Ex}$. Where $E_{Ex} \approx$ 0.24eV levels and $E_{Gap,Opt}$ were estimated from the onset of the solid state UV-Vis absorbance (**Figure S2**, **Table 1**).

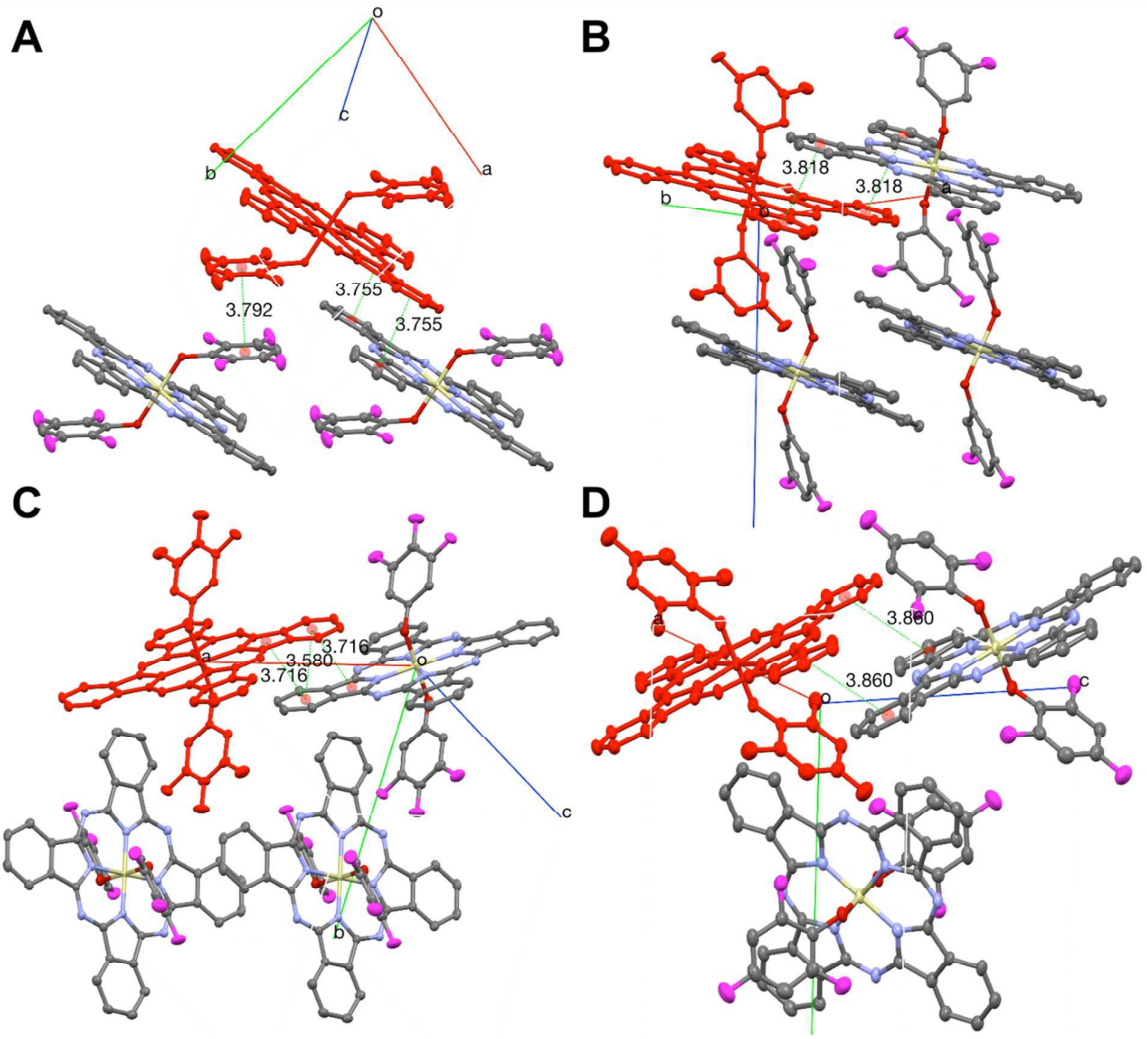

Figure 4 – Solid state arrangements of $(2356F)_2$-SiPc (**A**), and $(35F)_2$-SiPc (**B**), $(345F)_2$-SiPc (**C**) and $(246F)_2$-SiPc (**D**) obtained by single crystal X-ray diffraction. The dotted green lines represent molecular π-π interactions between neighboring molecules (< 4 Å). All crystals were grown from slow diffusion of heptane into a THF solution.

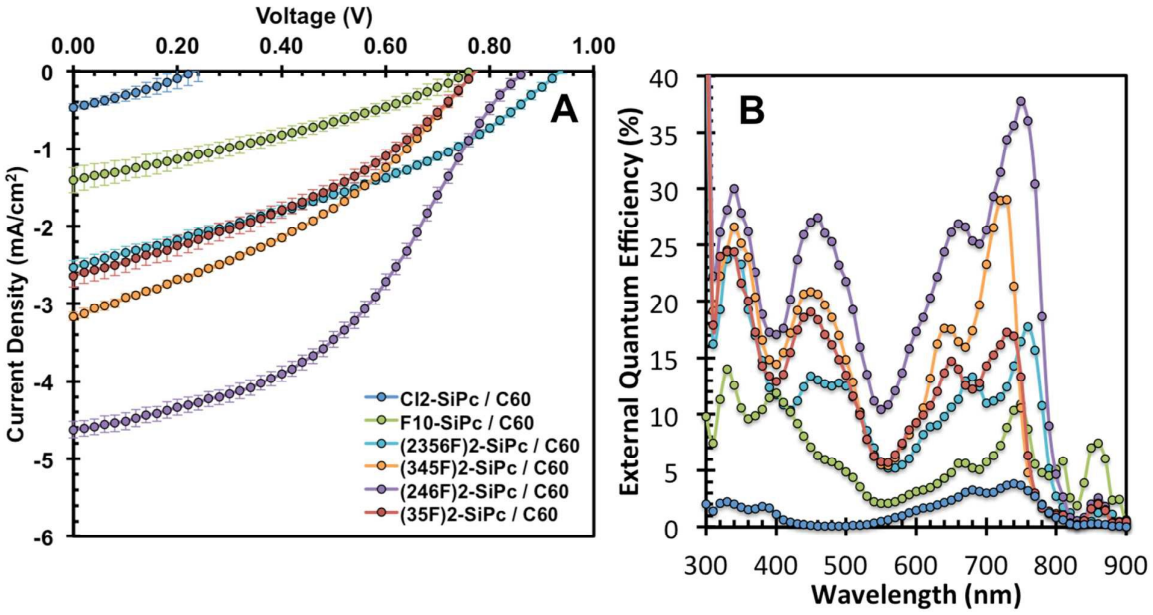

Figure 5. (**A**) J-V curves and (**B**) external quantum efficiency (% vs. nm) for a series of $(XF)_2$-SiPcs /C_{60} PHJ OPV devices. The legend in (**A**) is the same as for (**B**). The error bars represent the 95% confidence interval of the data set taken from an average of 6-10 devices over 3-4 substrates except device $(246F)_2$-SiPc/C_{60} which was replicated three additional times and the average was taken from 46 devices over 12 substrates.

Table 2. Organic photovoltaic (OPV) device structure and characterization

Device[a)]	Donor[b)]	Acceptor[b)]	V_{OC}[c)] (V)	J_{SC}[c)] (mA·cm^{-2})	FF[c)]	PCE[c)] (%)	REF
A	Cl_2-SiPc	C_{60}	0.24±0.05	0.5±0.1	0.32±0.03	0.04±0.01	[32]
B	F_{10}-SiPc	C_{60}	0.76±0.03	1.4±0.2	0.31±0.01	0.34±0.04	[32]
C	$(2356F)_2$-SiPc	C_{60}	0.94±0.02	2.5±0.2	0.35±0.01	0.83±0.07	This work
D	$(345F)_2$-SiPc	C_{60}	0.77±0.01	3.2±0.1	0.37±0.01	0.90±0.03	This work
E	$(246F)_2$-SiPc	C_{60}	0.87±0.03	4.6±0.4	0.44±0.02	1.8±0.2	This work
F	$(35F)_2$-SiPc	C_{60}	0.78±0.03	2.7±0.3	0.37±0.01	0.76±0.09	This work
G[d)]	Pentacene	Cl_2-SiPc	0.14±0.01	2.3±0.3	0.35±0.02	0.11±0.02	[32]
H[d)]	Pentacene	F_{10}-SiPc	0.41±0.01	2.4±0.2	0.45±0.02	0.45±0.03	[32]
I[d)]	Pentacene	$(2356F)_2$-SiPc	0.45±0.01	1.3±0.1	0.32±0.02	0.19±0.02	This work
J[d)]	Pentacene	$(345F)_2$-SiPc	0.51±0.02	1.2±0.1	0.46±0.06	0.29±0.05	This work
K[d)]	Pentacene	$(246F)_2$-SiPc	0.61±0.01	0.9±0.1	0.62±0.05	0.32±0.03	This work
L[d)]	Pentacene	$(35F)_2$-SiPc	0.54±0.01	0.9±0.1	0.62±0.03	0.29±0.03	This work
M	α-6T	Cl_2-SiPc	0.29±0.02	1.2±0.1	0.39±0.04	0.13±0.02	[32]
N	α-6T	F_{10}-SiPc	0.41±0.02	2.7±0.2	0.36±0.01	0.40±0.04	[32]
O	α-6T	$(2356F)_2$-SiPc	0.56±0.04	2.1±0.1	0.40±0.03	0.48±0.06	This work
P	α-6T	$(345F)_2$-SiPc	0.66±0.09	3.5±0.4	0.43±0.08	1.0±0.2	This work
Q	α-6T	$(246F)_2$-SiPc	0.65±0.01	2.3±0.1	0.583±0.02	0.87±0.03	This work
R	α-6T	$(35F)_2$-SiPc	0.58±0.01	2.0±0.1	0.33±0.01	0.37±0.01	This work

[a)] Device structure: ITO/PEDOT:PSS/Donor/Acceptor/BCP/Ag(80 nm). [b)]For device A-F: acceptor = 20 nm and donor = 40 nm; device G-L: acceptor = 43nm and donor = 40 nm; device M-R: acceptor = 60nm and donor = 20 nm. [c)] Device characteristics taken from an average of 12-18 pixels over 3-4 devices except device E and P which were replicated three additional times and the average was taken from 46 pixels over 12 devices. The +/- is the standard deviation of this data set. [d)] All devices were done with BCP = 7.5 nm except device G-L, which were done with BCP = 11 nm.

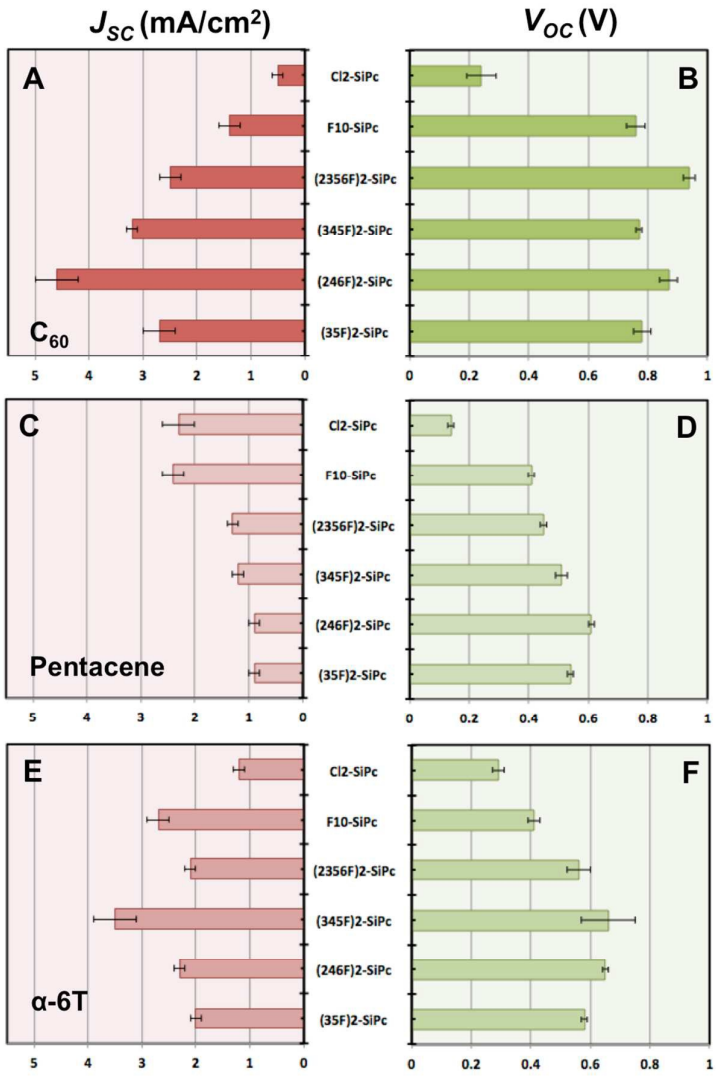

Figure 6. J_{SC} (Left) and V_{OC} (right) for a series of α-6T/$(XF)_2$-SiPc (A and B), pentacene/$(XF)_2$-SiPc (C and $(XF)_2$-SiPc/C_{60} (E and F) containing PHJ OPV devices. Tabulation of the values and error bars (standard deviation) can be found from **Table 2**.

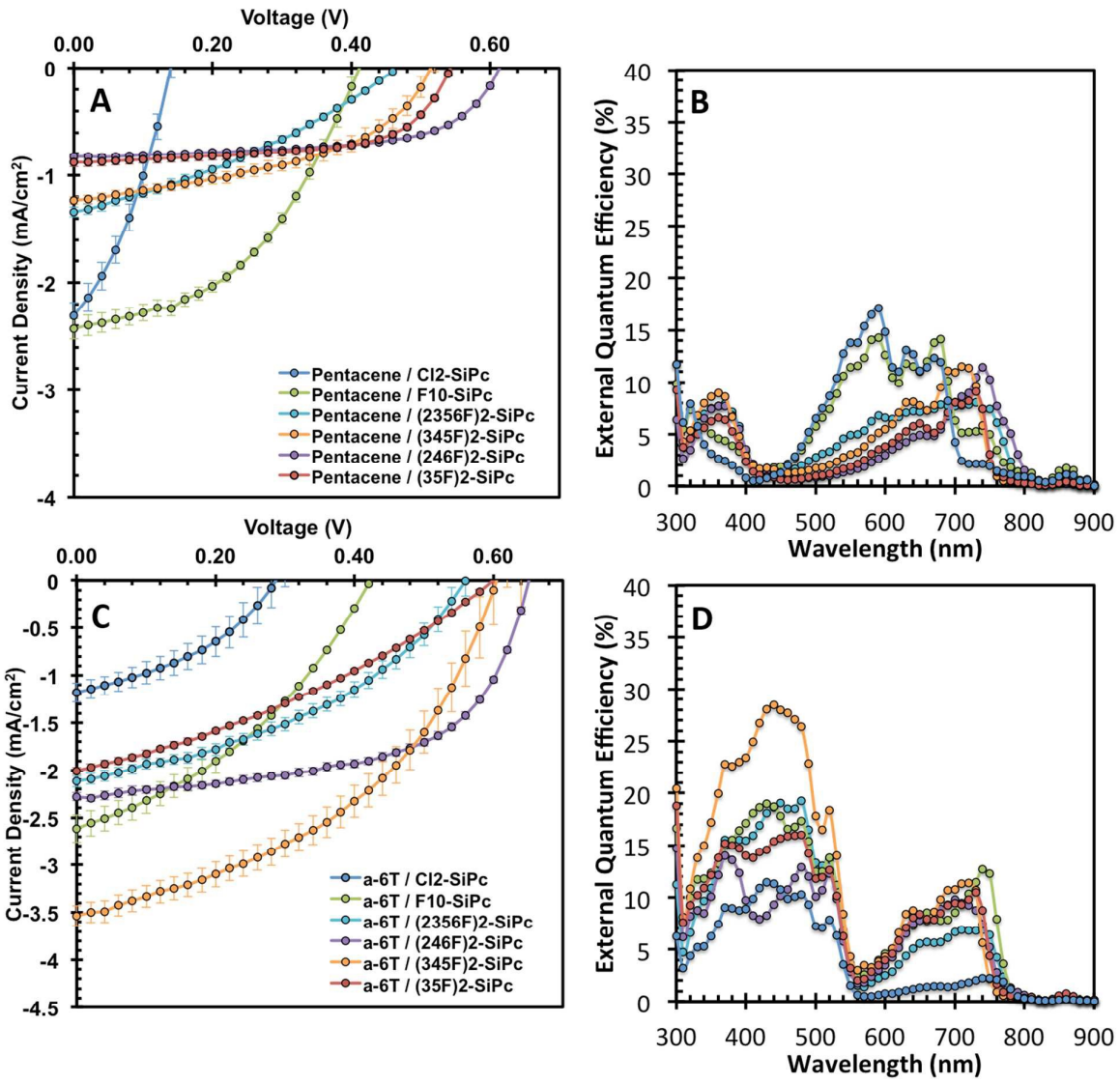

Figure 7. A), C) J-V curves and B), D) external quantum efficiency (% vs. nm) for a series of pentacene/$(XF)_2$-SiPc (A and B) and α-6T/$(XF)_2$-SiPc (C and D) PHJ OPV devices. The legend in A) is the same as for B), while the legend in C) is the same as in D). The error bars represent the 95% confidence interval of the data set taken from an average of 6-10 pixels over 3-4 devices except device a-6T/345-SiPc which was replicated three additional times and the average was taken from 46 pixels over 12 devices

For use in table of content only.

The Position and Frequency of Fluorine Atoms Changes the Electron Donor/Acceptor Properties of Fluorophenoxy Silicon Phthalocyanines within Organic Photovoltaic Devices

Benoît H. Lessard,[1,†] Trevor M. Grant,[1] Robin White,[2] Emmanuel Thibau,[2] Zheng-Hong Lu[2] and Timothy P. Bender,[1,2,3,]*